Non-Contact Inclusion Detection in Food through a Single-Photon Time-of-Flight Imager

Rudi Lussana, Federica Villa, *Member, IEEE*, Alberto Dalla Mora, Davide Contini, Andrea Farina, Laura Di Sieno, and Franco Zappa, *Senior Member, IEEE*

***Abstract* — We present a non-contact and non-invasive Diffuse Optical Imaging (DOI) system, based on an array of 32 × 32 Single-Photon Avalanche Diodes (SPADs) and Time-to-Digital Converters (TDCs), able to measure the Time-of-Flight (ToF) of single-photons, with 350 ps resolution. Measurements using Continuous-Wave (CW) and Time-Domain (TD) techniques demonstrate the possibility to identify the presence of absorbing inclusions (not visible by eye because of high scattering) within a diffusive media in transmittance geometry, with no contact with the sample. Thanks to the 1024 fully-independent and concurrent time-resolved detection points, TD acquisitions achieve better resolution than CW ones, with the same measurement time. Provided that the investigated medium presents adequate thickness and transmissivity at the wavelengths of interest in order to allow sufficient light penetration, the system can be employed as a quick imaging device in food industries for non-destructive quality control.**

***Index Terms* — Single-Photon Avalanche-Diode (SPAD); Time-to-Digital Converter (TDC); Photon timing, Photon counting, Diffusive Optical Imaging (DOI); Time-of-Flight (ToF).**

I. Introduction

Quality control in food industries has to comply ever more stringent rules and it can benefit from the exploitation of non-invasive, non-contact and fast techniques for product monitoring. Among others, optical methods are the best candidates to achieve this goal, since they involve neither direct contact with the sample nor food contamination. In particular, Diffusive Optical Imaging (DOI) allows to probe scattering media, such as meat, fruit, milk, etc., not only on the surface, but also in depth [1], [2].

Different approaches can be explored for food quality assessment, with different aims. One approach makes use of spectroscopy to identify the percentage of food components (e.g., water, lipid, chlorophyll) and to characterize even the fruit ripening level, based on the chlorophyll concentration [3], [4]. In that case, a single source-detector pair is placed on the external surface, and the light-probed volume is limited to the classical "banana shape" subtended by source and detector [5]. Instead, multiple measurement points, e.g. along the fruit circumference, are required to assess the possible presence of internal defects with higher absorption level with respect to the rest of the sample. In this way, a complete reconstruction of the entire fruit volume is possible by means of tomographic approaches [6] (exploiting multiple source-detector couples placed on the sample surface or a single detector coupled to a raster scanner) by constructing a sensitivity matrix based on analytical, numerical or experimental methods. The inverse problem is then solved to retrieve the perturbation position inside the sample. Besides high computational costs, this approach requires the construction of a mesh representing the sample geometry.

Another technique is to exploit DOI. In this case, a trans-illuminated or reflectance image is acquired through scanning or wide-field approach [7], [8]. If a reference image is available, the comparison with the sample image enables a fast localization of the inhomogeneity on the x-y plane, with no need for complex analysis algorithms. Moreover, if inhomogeneity composition data is required, it is also possible to acquire spectral information through hyperspectral acquisitions. A further data dimension can be explored by collecting the photon's time-of-flight (ToF) information, since "early" and "late" photons hitting the detector carry different information on the sample. In fact, in diffusive media, high spatial frequencies are dumped less at early times than at late ones [9], thus affecting image resolution.

From all these considerations, we can conclude that devices capable of measuring the ToF of a light pulse travelling through a diffusive media can be profitably exploited in prompt food-quality control for detecting the presence of contaminants. In particular, the availability of sensors capable of counting and time-stamping the arrival time of single photons with sub-nanosecond resolution allows to minimize active illumination power and improve system resolution when operating with relatively small inclusions. A candidate sensor is an intensified CCD camera although, besides high pixel resolution and good gating properties, it does not allow to directly measure photons' ToF. Instead, in this paper we present a system based on a 32 × 32 Single-Photon Avalanche-Diode (SPAD) camera with a 350 ps-resolution

R. Lussana, F. Villa, A. Tosi and F. Zappa are with the Dipartimento di Elettronica, Informazione e Bioingegneria, Politecnico di Milano, Milano 20133, Italy (e-mail: franco.zappa@polimi.it).

A. Dalla Mora, D. Contini and L. Di Sieno are with the Dipartimento di Fisica, Politecnico di Milano, piazza Leonardo Da Vinci 32, Milano 20133, Italy.

A. Farina is with the Istituto di Fotonica e Nanotecnologie, Consiglio Nazionale delle Ricerche, Milano 20133, Italy.

Time-to-Digital Converter (TDC) integrated into each pixel, for fast non-contact time-domain DOI. When dealing with diffusive media, the relatively low lateral resolution of just 32 × 32 pixels does not limit image quality, because high spatial frequencies are shortly dumped during the propagation. Moreover, compared to Ref. [10] where only 32 TDCs were integrated into a 128 × 128 SPAD array, we conceived the camera with one TDC per pixel, in order to provide 1024 fully-independent and concurrent detection points for single-photon counting and timing.

The presence of heterogeneities can be revealed by the loss of photons whose path intersects the inhomogeneity, thus giving a contrast as a function of the ToF. Our approach is similar to the one presented in Ref. [11], but it is applied to absorbing inclusions instead of reflecting ones and furthermore we operate in transmission mode, aiming at identifying in-homogeneities along the whole sample thickness.

Section II describes the system and the sample under test, while data analysis is discussed in *Section III*. *Section IV* concludes the paper and opens the way to future research.

II. Experimental set-up

The main building blocks of our experimental set-up are a collimated high-power picosecond pulsed laser, a diffusive medium (in our case a commercially-available yogurt) with and without an absorbing inclusion (mimicking an insect or packaging debris), and the 32 × 32 pixels time-resolved SPAD camera (see Fig. 1).

A. Optical laser source

We employed a four-wave-mixing laser source at 743 nm-wavelength with Full-Width-Half-Maximum (FWHM) lower than 100 ps, 40 MHz repetition rate and 90 mW average power. At the free-space output we placed a neutral density variable attenuator to adjust the optical power, in order not to distort the measurement by keeping the photon detection probability lower than 5% [12]. Then, the laser beam was focused on the input surface of the sample.

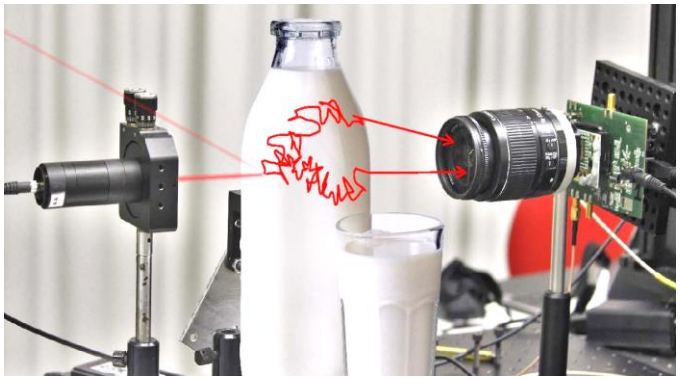

Fig. 1. Concept of the measurement: the sample under test is placed between laser source and 35 mm-objective put in front of the 32x32 SPAD+TDC camera.

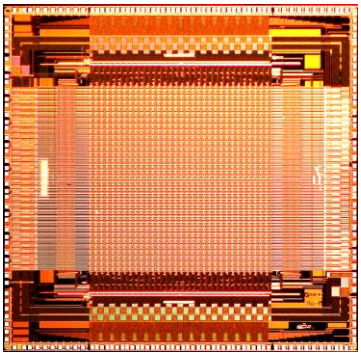

Fig. 2. Micrograph of the 32 × 32 array with 1024 SPADs and 1024 TDCs.

B. Sample

As diffusive medium we analyzed a common commercially-available yogurt, after measuring its optical properties by means of the instrument described in Ref. [13], across the 600 – 1100 nm range. At the 743 nm-measurement wavelength the absorption coefficient is 0.03 cm^{-1} and the reduced scattering coefficient is about 36 cm^{-1}. Usually, liquid phantoms for DOI are composed by a mixture of Intralipid-20% as diffusive medium and ink as absorber in a distilled water dilution [14]. Here we preferred to use a common industrial product, not specific for research purpose, aiming at demonstrating the direct applicability of out technique to non-destructive quality control in industry applications.

The 50 ml yogurt was inside a 25 cm^2 transparent 2 cm-thick polystyrene flask. The absorbing inclusion was a small (about 3 × 3 × 3 mm^3) scrap of black neoprene, positioned in the center of the flask and not visible by eye from any point of view. Following Ref. [15] and Ref. [16], the perturbation produced by this totally absorbing object can be estimated in less than 0.06 cm^{-1} within a 1 cm^3 volume.

C. SPAD plus TDC sensor

A micrograph of the SPAD imager is shown in Fig. 2. The chip, developed in a 0.35 µm standard CMOS technology, integrates 32 × 32 independent channels, each including a 30 µm-diameter SPAD and a 350 ps-resolution TDC.

The array can be operated in two modalities: *photon counting* (i.e. each pixel counts the number of photons detected therein) and *photon timing* (i.e. each pixel time-stamps the first photon detected therein in each frame, by measuring its arrival time through the in-pixel TDC). The former can be used to acquire 2D intensity images of the sample, up to 100,000 frames/s; the latter to gather the 2D map of ToF information.

The imager is described and characterized in detail in Ref. [17] and its performance is summarized in TABLE I. The Photon Detection Efficiency (PDE) tops at 55% at 450 nm, dropping down to 12% at the 743 nm laser's wavelength. The Dark Count Rate (DCR) normalized to the active area is significantly lower than the one achieved by other SPAD+TDC arrays developed in more scaled technologies[18], [19], whereas excellent TDC linearity performance (2% LSB DNL, 10% LSB INL) is achieved thanks to the sliding-scale technique [20].

TABLE I. PERFORMANCE OF THE SPAD + TDC ARRAY.

Parameter	*Value*	*Units*
Pixel number	32 × 32	
SPAD diameter	30	µm
Fill-factor (FF)	3.14	%
Peak Photon Detection Efficiency (PDE) @ 450 nm	55	%
Photon Detection Efficiency (PDE) @ 732 nm	12	%
Dark Count Rate (DCR) @ room temperature	120	cps
Dynamic Range (DR) @100 fps [21]	95	dB
TDC Least Significant Bit (LSB)	350	ps
TDC Full Scale Range (FSR)	360	ns
Overall precision (σ)	280	ps
Differential Non-Linearity (DNL) rms	2	% LSB
Integral Non-Linearity (INL) rms	10	% LSB
Maximum frame-rate	100,000	frame/s
Power consumption	400	mW

III. MEASUREMENTS AND RESULTS

We performed two different measurement campaigns, to study the diffusive medium behavior: at first, we measured the intensity (photon counting) of the light crossing the medium, without recording the detected photons arrival time (i.e. similarly to a CW technique); then we exploited the photon timing feature of the imager, by acquiring the ToF of single photons diffusing through the sample (i.e. performing a TD measurement). In both cases, we also acquired a reference measurement of the medium without heterogeneity. In the followings, we define contrast as the log_{10} of the ratio between unperturbed (homogeneous) and heterogeneous (with unwelcome inclusion) measurements.

Note that the reported Time-of-Flight values do not relate to the straight line optical path between laser source and SPAD pixel, but to the overall optical path travelled by the photon inside the diffusive media, after very many scattering events.

A. *Continuous-Wave photon counting acquisition*

The sample was illuminated by the laser source, and the SPAD camera counted the number of detected photons in 100 s-integration time, with a Field-of-View (FoV) of 5 × 5 cm^2. The 100 s integration time was chosen in order to collect at least 1000 photons even on the least illuminated pixels in the perturbed acquisition.

Since the absorbing inclusion creates shadows and reduces the number of photons successfully passing through the medium, we compared the intensity images obtained with homogeneous and perturbed sample, after two acquisitions of the same duration and with the same total optical power. Fig. 3 shows the total number of acquired photons per each pixel (i.e. the 32 × 32-pixel intensity map) of the homogeneous (a) and heterogeneous medium (b), in which pixels on the direct laser path show a higher photon count rate.

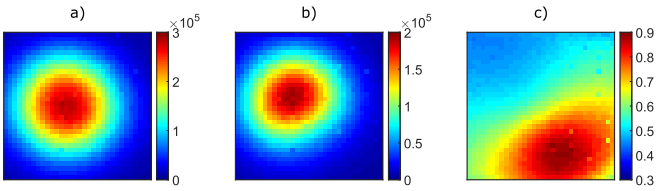

Fig. 3. Intensity image showing the total number of photons detected in the 100 s integration window for both homogeneous (a) and perturbed (b) diffusive medium, and resulting contrast map (c), obtained as the log10 of the ratio between photons detected by the SPAD imager in the two conditions. The perturbation is localized in the bottom-right corner of the flask, in correspondence of the peak in the contrast value, which reaches 0.9 and covers an area of 376 pixels (FWHM). The inclusion was located at 1 cm depth.

Then, Fig. 3 (c) shows the contrast map from which the inclusion (localized in the bottom-right corner of the flask, at 1 cm depth) is clearly identifiable in the bottom-right corner, in correspondence of a peak in the contrast map (covering 376 pixels at FWHM).

B. *Time-Domain photon timing acquisition*

In the second approach, we performed a TD acquisition exploiting the photon timing mode of the SPAD camera, for assessing the time-resolved transmittance curve variations between homogeneous and heterogeneous samples. As for CW measurements, the integration time for each acquisition was 100 s and the FoV was 5 × 5 cm^2. The 100 s acquisition duration was chosen in order to guarantee the same operating conditions as for the CW measurement.

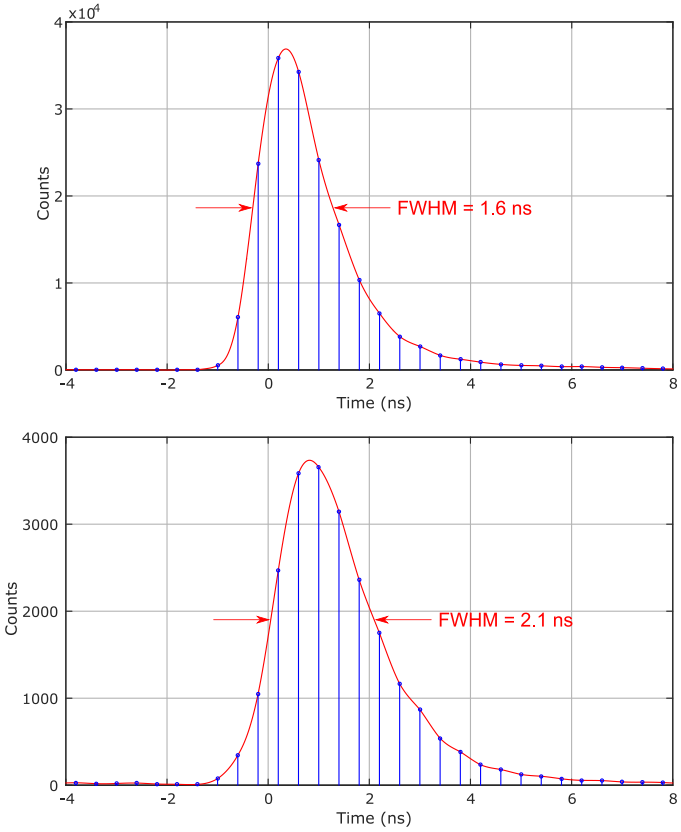

Fig. 4 ToF distributions acquired by two pixels of the array on a homogeneous sample: central pixel (top) near the inclusion exhibit a narrower pulse shifted towards early time if compared to lateral pixel (bottom).

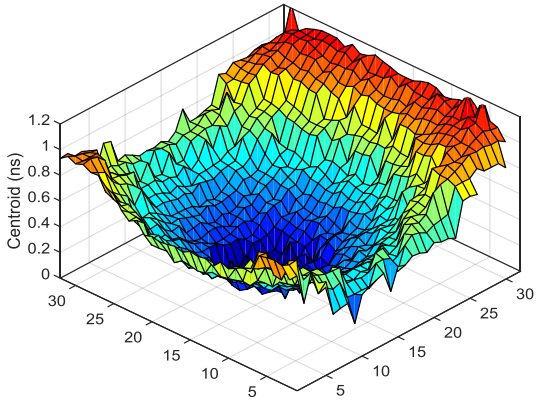

Fig. 5. ToF centroids distribution map for each array pixel, normalized to the shortest arrival time.

Again, as homogeneous measurement we acquired the 32 × 32-pixel ToF map with yogurt alone and we built the ToF histograms, as shown in Fig. 4 for two representative pixels. As well-known from theory [22], the ToF distribution detected by a pixel on-axis to the injection point (Fig. 4 top) is narrower and shifted toward early-times compared to an off-axis pixel (Fig. 4 bottom), due to the longer average photon path between source and detector in the case of off-axis pixels. This behaviour is highlighted in the ToF centroids map shown in Fig. 5: about 1 ns-time time shift results between on- and off-axis pixels.

Then we inserted the absorbing inclusion in the sample and we repeated the same acquisition. As for the CW case, no difference between unperturbed and perturbed situations can be observed by eye in the histograms. So we performed again the previous analysis, by computing the contrast for each pixel and ToF time.

The impact of the heterogeneity on the resulting histogram depends on pixel position: Fig. 6 shows the contrast, as defined in Sect. III, for two different pixels, on- and off-axis, respectively. The contrast intensity depends on both inclusion size and optical properties of the diffusive media: in particular, large inclusions in highly diffusive media introduce a strong attenuation [15][16], especially on early photons, thus causing a high contrast at early time. With the setup described in

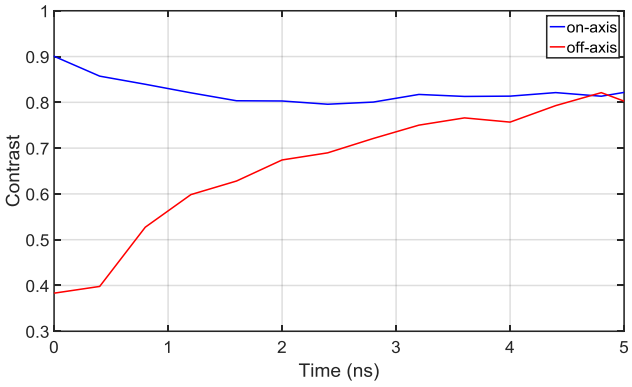

Fig. 6. Contrast as a function of photons arrival time, for both on- (blue curve) and off-axis (red curve) pixels. At longer ToFs, the contrast is slightly decreasing for on-axis pixels and increasing for off-axis ones.

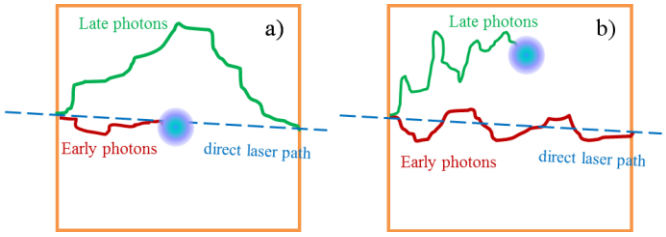

Fig. 7. Exemplification of paths travelled by “early” and “late” photons, for both on-axis (a) and off-axis (b) pixels.

Sect. II, for the on-axis pixel the contrast is about 0.9 for short ToF, decreasing down to 0.8 in about 1.5 ns; for the off-axis pixel, instead, the contrast is increasing for longer ToF [15].

In the case highlighted in Fig. 7 (a), the laser source, inclusion and detection points are aligned. At early ToFs, the number of paths connecting source and detector is low and these paths are mainly concentrated on the source-detector axis. This causes a higher contrast at early times. Instead, for later arrival times, the number of possible paths increases and also the number of trajectories crossing the inclusion proportionally increase, hence contrast becomes almost constant.

The opposite situation, in which the inclusion is off-axis, is sketched in Fig. 7 (b): late photons are those with higher probability on average to be absorbed by the inclusion, thus giving a high contrast at late times. On the contrary, early photons are not influenced on average by the inclusion, thus giving a very low contrast.

In conclusion when laser source, inclusion and detecting pixel are aligned, early photons experience higher absorption probability, whereas late photons have higher probability to pass the obstacle without being absorbed. Vice versa, when they are not aligned, early photons have higher probability to be left unperturbed, while late photons experience higher probability of reaching the perturbation.

Since the SPAD camera can provide ToF data from all pixels on a frame-by-frame basis, it is possible to acquire a real-time movie of the ToF maps. Fig. 8 shows the contrast acquired in the same conditions of Fig. 3, at four different frames captured at different photons arrival times, moving from early (a) to late (d) photons. As expected from previous discussions, the localization of the perturbation is better at early times, while the lateral resolution degrades at longer ToF delays. In particular, the contrast maps presents a peak covering an area of 184 pixels for Fig. 8 (a), and broadening for later arrival times, covering 324, 391 and 394 pixels for Fig. 8 b, c and d, respectively.

IV. Discussion

Considering the results shown in Fig. 3 (c) and Fig. 8 (a), both CW and TD DOI allow to identify the presence of an inclusion inside the medium by simply comparing the homogeneous sample with the heterogeneous one. Nevertheless, with the same measurement duration and despite the use of a very simple analysis procedure, the TD

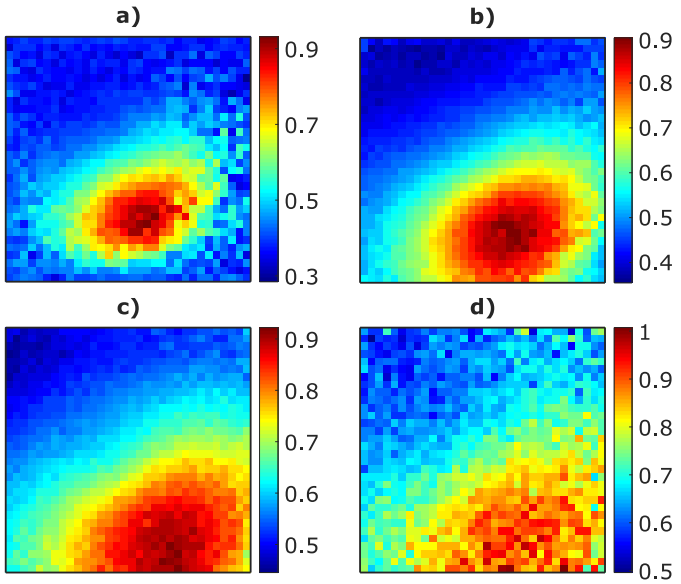

Fig. 8. Contrast images at different elapsed times from the laser pulse excitation: 400 ps (a), 1.2 ns (b), 2.8 ns (c) and 5.6 ns (d) after the detection of earliest photons. The inclusion is localized in correspondence of the high contrast values in the bottom right of the flask, with early photons (frames a and b) providing a better localization resolution with respect to late ones (frames c and d). In particular, the contrast maps in (a), (b), (c) and (d) cover a FWHM area of 184, 324, 391 and 394 pixels, respectively, providing better spatial resolution compared to the 376 pixels of Fig. 3 (c).

measurement presents a better spatial resolution. In fact, the 376 pixel peak in the CW acquisition of in Fig. 3 (c) is narrowed to just 184 pixels in Fig. 8 (a), thus allowing a better inclusion localization when only early arrival times are considered. The peak area then broadens up to 394 pixels when late photons are considered.

Both methods rely on the acquisition of a homogeneous image to be used as a reference, which can be performed just once on a reference sample, and does not require to be repeated for each successive acquisition with different samples.

Compared to the other techniques mentioned in *Section I*, thanks to the 32 × 32 SPAD imager employed, we were able to conduct relatively fast measurements (100 s), with no need of complex post processing and inverse problem solution. The drawback is the impossibility to locate the inclusion positions along the z axes, but only in *x-y* plane. Using a tomographic approach with multiple acquisitions at different observation angles and with some post processing (see for example Ref. [11]), it will be possible to identify the position of the inclusion across the 3D x-y-z space; this will be object of a future work.

The 100 s acquisition time was mainly limited by the data transfer to the computer for the analysis, with the bottleneck set by the USB 2.0 link we employed; in fact, the throughput capability of the 32 × 32 SPAD+TDC imager itself is about a factor 10x better. A novel camera is currently under development, employing the same SPAD chip, but with a USB 3.0 link, which will reduce the acquisition time to about 11 s.

V. Conclusions

In this paper we reported the proof-of-concept of a system based on a 32 × 32 Time-of-Flight single-photon avalanche-diode camera with in-pixel SPADs and time-to-digital converters, for non-contact and non-destructive localization of heterogeneities inside food. In particular, we focused this work on the detectability of a totally absorbing object (similar to an insect or package debris) not visible by eye due to the high scattering within a commercial yogurt. Thanks to the fully concurrent approach, there is no need of long scanning of the object, thus keeping the measurement time low. The camera can be operated both in photon counting and in photon timing modes (350 ps resolution) for performing either continuous wave analysis or time-domain investigations. Thanks to the 1024 fully-parallel ToF sensitive pixels, the time-domain approach achieves better resolution with the same measurement duration.

For our proof-of-concept analysis, we employed yogurt, however the technique applies in principle also to cheeses, creams, fruits and other food, provided that the medium has adequate thickness and transmissivity at the wavelengths of interest in order to allow sufficient light penetration. Additionally, when the sample cannot be investigated in transmittance geometry, similar techniques can be in principle applied in reflectance geometry, thus allowing to probe the sample down to a depth of few centimeters from all sides. Therefore, results are relevant for industries to disclose impurities in foods.

References

[1] Y. Zhai, S. A. Cummer, “Fast tomographic reconstruction strategy for diffuse optical tomography,” *Opt. Express*, vol. 17 no.7, pp. 5285–5297, 2009.

[2] A. Yodh and B. Chance, "Spectroscopy and imaging with diffusing light," *Phys. Today*, vol. 48 no. 3, pp. 34–41, 1995.

[3] R. Cubeddu, C. D’Andrea, A. Pifferi, P. Taroni, A. Torricelli, G. Valentini, M. Ruiz-Altisent, C. Valero, C. Ortizl, C. Dover, D. Johnson, and C. Ortiz, "Time-Resolved Reflectance Spectroscopy Applied to the Nondestructive Monitoring of the Internal Optical Properties in Apples," *Appl. Spectrosc., vol.* 55, no. 7, pp. 1368–1374, 2001.

[4] A. Torricelli, L. Spinelli, J. Kaethner, J. Selbeck, A. Franceschini, P. Rozzi, and M. Zude, "Non-destructive optical assessment of photon path lengths in fruit during ripening: implications on design of continuous-wave sensors," in *International Conference Of Agricultural Engineering*, 2012.

[5] T. Durduran, R. Choe, W. B. Baker, andA G Yodh, “Diffuse optics for tissue monitoring and tomography,” *Rep. Prog. Phys.*, vol. 73, no. 7, 076701, 2010.

[6] E. K. Kemsley, H. S. Tapp, R. Binns, R. O. Mackin, and A. J. Peyton, "Feasibility study of NIR diffuse optical tomography on agricultural produce," *Postharvest Biol. Technol., vol.* 48, no. 2, pp. 223–230, 2008.

[7] Spinelli L, Torricelli A, Pifferi A, Taroni P, Danesini G, Cubeddu R. “Characterization of female breast lesions from multi-wavelength time-resolved optical mammography,” *Phys Med Biol.* 2005; vol.50, no. 11, pp. 2489–2502, 2005.

[8] D. J. Cuccia, F. Bevilacqua, A. J. Durkin, and B. J. Tromberg, "Modulated imaging: quantitative analysis and tomography of turbid media in the spatial-frequency domain.," *Opt. Lett., vol.* 30, no. 11, pp. 1354–1356, 2005.

[9] A. Bassi, C. D’Andrea, G. Valentini, R. Cubeddu, and S. Arridge, "Temporal propagation of spatial information in turbid media.," *Opt. Lett., vol.* 33, no. 23, pp. 2836–2838, 2008.

[10] J. M. Pavia, M. Wolf, E. Charbon, "Single-photon avalanche diode imagers applied to near-infrared imaging," *IEEE Journal on Selected Topics in Quantum Electronics*, vol. 20, no. 6, 2014.

[11] J. Pichette, S. Boucher, G. B. Domínguez, Y. Bérubé-Lauzière, "Diffuse photon density wavefront speed as a contrast for tomographic imaging of heterogeneous diffusive media," *Optics Letters*, vol. 39, no. 7, pp. 2097–2100, 2014.

[12] D. O'Connor and D. Phillips, "Time-correlated single photon counting", Academic Press, London, 1984.

[13] S. Konugolu Venkata Sekar, A. Dalla Mora, I. Bargigia, E. Martinenghi, C. Lindner, P. Farzam, M. Pagliazzi, T. Durduran, P. Taroni, A. Pifferi, and A. Farina, "Broadband (600-1350 nm) Time Resolved Diffuse Optical Spectrometer for Clinical Use," *IEEE J. Sel. Top. Quantum Electron.*, vol. 22, no. 3, pp. 406–414, 2016.

[14] L. Spinelli, F. Martelli, A. Farina, A. Pifferi, A. Torricelli, R. Cubeddu, and G. Zaccanti, "Calibration of scattering and absorption properties of a liquid diffusive medium at NIR wavelengths. Time-resolved method," *Opt. Express*, vol. 15 no. 11, pp. 6589–6604, 2007.

[15] F. Martelli, A. Pifferi, D. Contini, L. Spinelli, A. Torricelli, H. Wabnitz, R. Macdonald, A. Sassaroli, and G. Zaccanti, "Phantoms for diffuse optical imaging based on totally absorbing objects, part 1: Basic concepts," *J. Biom. Opt.*, vol. 18, no. 1, 66014, 2013.

[16] F. Martelli, P. Di Ninni, G. Zaccanti, D. Contini, L. Spinelli, A. Torricelli, R. Cubeddu, H. Wabnitz, M. Mazurenka, R. Macdonald, A. Sassaroli, and A. Pifferi, "Phantoms for diffuse optical imaging based on totally absorbing objects, part 2: experimental implementation," *J. Biomed. Opt.*, vol. 19, no. 7, 076011, 2014.

[17] F. Villa, "CMOS imager with 1024 SPADs and TDCs for single-photon timing and 3D time-of-flight," *IEEE J. Sel. Top. Quantum Electron.*, vol. 20, no. 6, 2014.

[18] C. Veerappan, J. Richardson, R. Walker, D. Li, M.W. Fishburn, et al. "A 160×128 Single-Photon Image Sensor with On-Pixel 55ps 10b Time-to-Digital Converter", *IEEE Int. Solid-State Circuits Conf.*, 2011.

[19] M. Gersbach, Y. Maruyama, E. Labonne, J. Richardson, R. Walker, et al., "A parallel 32×32 time-to-digital converter array fabricated in a 130 nm imaging CMOS technology," *ESSCIRC 2009 - Proceedings of the 35th European Solid-State Circuits Conf.*, pp. 196–199, 2009.

[20] F. Villa, B. Markovic, S. Bellisai, D. Bronzi, A. Tosi, et al. "SPAD Smart-Pixel for Time-of-Flight and Time-Correlated Single-Photon Counting Measurements," *Photonic Journal*, vol. 4, no. 3, pp. 795–804, 2012.

[21] D. Bronzi, F. Villa, S. Tisa, A. Tosi, F. Zappa, "SPAD Figures of Merit for Photon-Counting, Photon-Timing, and Imaging Applications: A Review," *IEEE Sensors Journal*, vol. 16, no. 1, pp. 3–12, 2016.

[22] D. Contini, F. Martelli, and G. Zaccanti, "Photon migration through a turbid slab described by a model based on diffusion approximation. I. Theory," *Appl. Opt.*, vol. 36, no. 19, pp. 4587–4599, 1997.